UC Berkeley

UC Berkeley Previously Published Works

Title

Sum frequency generation (SFG) - Surface vibrational spectroscopy studies of buried interfaces: Catalytic reaction intermediates on transition metal crystal surfaces at high reactant pressures; Polymer surface structures at the solid-gas and solid-li...

Permalink

https://escholarship.org/uc/item/7ch3k68k

Journal

Applied Physics B: Lasers and Optics, 68(2-3)

ISSN

0946-2171

Authors

Chen, Z
Gracias, DH
Somorjai, GA

Publication Date

1999

DOI

10.1007/s003400050664

Copyright Information

This work is made available under the terms of a Creative Commons Attribution License, availalbe at https://creativecommons.org/licenses/by/4.0/

Peer reviewed

eScholarship.org Powered by the California Digital Library
University of California

Appl. Phys. B 68, 549–557 (1999)

Applied Physics B
Lasers
and Optics
© Springer-Verlag 1999

Invited paper

Sum frequency generation (SFG) – surface vibrational spectroscopy studies of buried interfaces: catalytic reaction intermediates on transition metal crystal surfaces at high reactant pressures; polymer surface structures at the solid–gas and solid–liquid interfaces

Z. Chen, D.H. Gracias, G.A. Somorjai

Department of Chemistry, University of California, Berkeley, CA 94720, and Materials Science Division, Lawrence Berkeley National Laboratory, Berkeley, CA 94720, USA
(Fax: +1-510/643-9668, E-mail: somorjai@socrates.berkeley.edu)

Received: 20 September 1998

Abstract. SFG has been utilized to monitor the surface species present on platinum and rhodium crystal surfaces during catalytic reactions at atmospheric pressures. Ethylene hydrogenation to ethane, cyclohexene hydrogenation to cyclohexane and its dehydrogenation to benzene, and carbon monoxide oxidation to carbon dioxide have been studied while also measuring the turnover rates and the gas phase product distribution by gas chromatography. Strongly bound spectators, weakly bound reaction intermediates, and pressure-dependent changes in the chemical bonding of surface species have all been observed.

SFG spectra of polyethylene and polypropylene show monolayer sensitivity and reveal temperature-dependent changes of surface structure. For polymer blends, the hydrophobic component segregates to the solid–air interface, and the hydrophilic component segregates at the solid–water interface. Changes in SFG spectra of polymer blends as a function of bulk concentration correlate with changes of contact angle. SFG is an excellent probe of surface-structure and surface-composition changes as the polymer interface is altered.

PACS: 68; 82.65.-i; 82.65.Jv

Surface scientists have modeled heterogeneous catalytic reactions on metal surfaces for 30 years, using a variety of techniques, which include low-energy electron diffraction (LEED) for surface crystallography, high-resolution electron energy loss spectroscopy (HREELS) and reflection adsorption infrared spectroscopy (RAIRS) for probing vibrational modes, Auger electron spectroscopy (AES) and X-ray photoemission spectroscopy (XPS) for chemical analysis of the surface, and mass spectrometry for monitoring the desorption of the surface species [1, 2]. Unfortunately all these methods require ultra-high vacuum (UHV) and the surface observed under UHV conditions is not necessarily the same as that present during a chemical reaction. Infrared-visible sum frequency generation (SFG), a surface-specific nonlinear optical spectroscopy [3–6] has recently been used to study the transition-metal surfaces over a wide range of temperatures (120–250 K) and pressures (UHV to atmosphere). These studies have bridged the gap between surface phenomena monitored in UHV and relevant reaction pressures [7].

Polymer surfaces have been extensively studied for many years by using many different techniques such as IR, Raman spectroscopy, XPS, contact angle measurement and atomic force microscopy (AFM) [8–11]. Some of these techniques require UHV, others are either not surface sensitive or cannot provide surface information at the molecular level. SFG can provide detailed information of polymer surfaces at the molecular level and can be used to study any polymer surface or interface that can be accessed by light.

SFG, a three-wave mixing process, is generated through the beating of input infrared (ω_{ir}) and visible (ω_{vis}) beams to produce an output at the sum frequency ($\omega_{\mathrm{sum}} = \omega_{\mathrm{ir}} + \omega_{\mathrm{vis}}$). The visible beam is held at a fixed frequency while the infrared beam is tuned over the vibrational range of interest. The SFG experiment probes the second-order nonlinear susceptibility ($\chi^{(2)}$) and the signal can be expressed as $I \propto |(\chi^{(2)})|^2$. The macroscopic $\chi^{(2)}$ can be related to the molecular polarizability by:

$$\chi^{(2)}_{\mathrm{ijk}} = N \sum_{l,m,n} \langle (\hat{i}\cdot\hat{l})(\hat{j}\cdot\hat{m})(\hat{k}\cdot\hat{n})\rangle \alpha^{(2)}_{lmn}. \quad (1)$$

We are interested only in the resonant term of $\alpha^{(2)}_{lmn}$, which can be expressed by:

$$\alpha^{(2)\mathrm{R}}_{lmn} = \sum_q \frac{A_q}{(\omega_q - \omega_2 - \mathrm{i}\Gamma_q)} \Delta\rho_{gq} \,, \tag{2}$$

where

$$A_q = \frac{1}{2\omega_q} \frac{\partial\mu_n}{\partial Q} \frac{\partial\alpha^{(1)}_{lm}}{\partial Q} \,, \tag{3}$$

and $\Delta\rho_{gq}$ is the population difference between the ground and first excited states, and $\frac{\partial\mu_n}{\partial Q}$ and $\frac{\partial\alpha^{(1)}_{lm}}{\partial Q}$ are the change in dipole moment and change in polarizability with respect to position. Hence, SFG requires modes to be both IR and Raman active in order to be observed, which makes SFG a surface-sensitive technique.

The orientation of the surface CH_3 group can be obtained by using different polarizations of infrared, visible and sum-frequency beams to measure different components of $\chi^{(2)}$ [12–14]. $\chi^{(2)}_{YYZ}$ can be measured by *ssp* (SF, visible and IR) polarizations and $\chi^{(2)}_{YZY}$ with *sps*. For CH_3 symmetric stretch we can show that

$$\left|\frac{\chi^{(2)}_{YYZ}}{\chi^{(2)}_{YZY}}\right| = \left|\frac{\langle\cos^3\theta\rangle + 0.56\langle\sin^2\theta\cos\theta\rangle}{0.44\langle\sin^2\theta\cos\theta\rangle}\right| \,. \tag{4}$$

So the average angle between the molecular symmetry axis and the surface normal, θ can be obtained. The orientation of surface CH_2 groups can be measured in a similar fashion.

1 Experimental

All the catalytic reaction experiments were performed in a UHV/batch reactor system using Pt(111) or Rh(111) single-crystal surfaces (Fig. 1). The crystal was cut, polished, and oriented by using conventional procedures. The UHV system was pumped by a turbo pump and an ion pump and had a base pressure of less than 1×10^{-10} Torr. The crystal could be heated resistively to over 1300 K and cooled with liquid nitrogen to approximately 115 K. The UHV system was equipped with an electron gun for argon-ion bombardment, a retarding field analyzer for LEED and Auger, and a mass spectrometer. In addition, the chamber has two CaF_2 windows which were used to allow tunable IR and green light into the chamber and to allow sum-frequency light to go out to a photomultiplier tube.

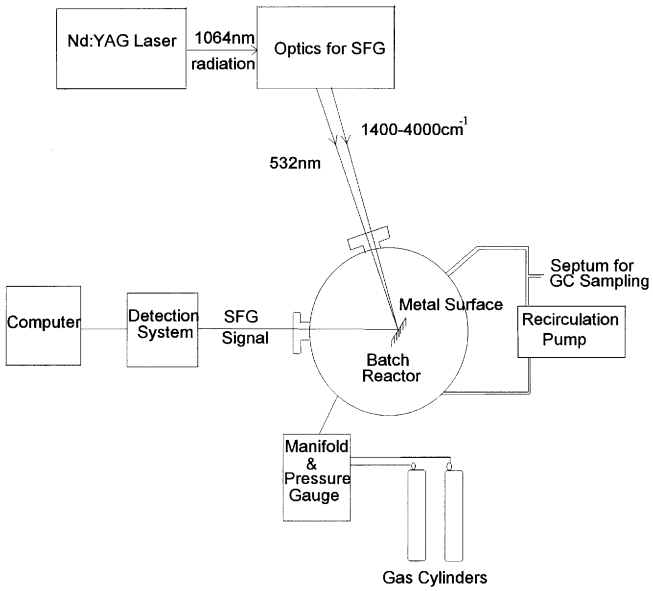

Fig. 1. The UHV/batch reactor apparatus for in situ catalysis

The SFG experiment is performed by overlapping a visible and a tunable IR beam on the sample surface at incident angles of 45° and 50°, respectively. The visible beam used is a small portion of the 532-nm output from a Continuum YAG-PY61 laser (generating ~ 20 ps pulses at 20 Hz). The IR beam, tunable from 2500 cm^{-1} to 3600 cm^{-1}, is generated from a combined OPG/OPA (optical parametric generation/optical parametric amplification) system composed of $LiNbO_3$ crystals pumped by the fundamental output of the YAG laser at 1064 nm. The SF output signal is collected by a gated integrator and photon counting system. The surface vibrational spectra are obtained by tuning the IR frequency and measuring the SF signal, with polarization combination of *ssp* (*s*-polarized SF output, *s*-polarized visible input and *p*-polarized IR input) or *sps*. The IR range can be expanded down to 1400 cm^{-1} by using $BBO/AgGaS_2$ OPG/DFG (DFG difference frequency generation) system.

A Rame–Hart NRL Contact Angle Goniometer was employed to measure the contact angle of liquids with known surface tension (water and methylene iodide) on polymer films, with the sessile drop technique [15]. XPS experiments were performed on a Perkin–Elmer PHI 5300 XPS spectrometer with a position sensitive detector and a hemispherical energy analyzer. The AFM used for imaging was a commercial Park Scientific M5 instrument. All the polymer samples were prepared by solvent casting from dilute solutions onto quartz substrates. The solvents used were O-xylene for polyethylene and polypropylene and *N*, *N*-Dimethylacetamide for the polymer blends.

2 Results and discussion

2.1 Ethylene hydrogenation [16, 17]

Three distinct spectroscopic features were seen on the Pt(111) surface during ethylene hydrogenation at 295 K with 100 Torr hydrogen and 35 Torr ethylene: di-σ bonded ethylene, π-bonded ethylene, and ethylidyne (Fig. 2a). When the reaction was carried out on an initially clean surface, the concentration of di-σ bonded ethylene that could be observed was about 8% of a monolayer. However, if the platinum surface was saturated with ethylidyne, very little di-σ bonded ethylene was observed under catalytic conditions (Fig. 2b) and the rate of hydrogenation (expressed by TOR, turn over rate), as measured by gas chromatography, was independent of the surface concentration of the di-σ bonded ethylene species. This is a strong argument against di-σ bonded ethylene being an important intermediate in ethylene hydrogenation. It is known from previous studies on supported catalyst surfaces that the presence or absence of ethylidyne has no affect on the rate of ethylene hydrogenation [18, 19]. The concentration

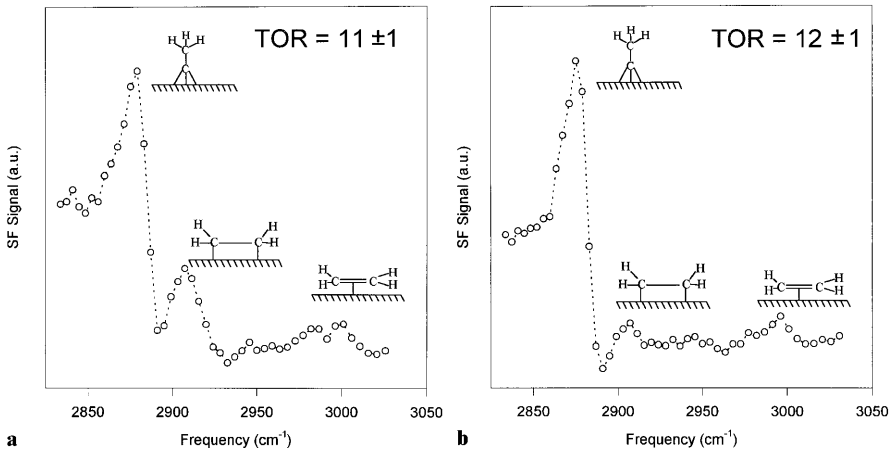

Fig. 2. a SFG spectrum of the Pt(111) surface during ethylene hydrogen with 100 Torr H_2, 35 Torr C_2H_4, and 615 Torr He at 295 K. **b** The SFG spectrum under the same conditions as (**a**), but on a surface which was precovered in UHV with 0.25 ML of ethylidyne

of π-bonded ethylene was unaffected by the ethylidyne concentration so that *the π-bonded species is likely to be a key intermediate in ethylene hydrogenation*.

The ethylene hydrogenation reaction was also carried out at higher pressures (723 Torr H_2, 38 Torr ethylene, and 295 K) and low pressures (1.75 Torr H_2, 0.25 Torr ethylene, and 758 Torr Ar) of hydrogen and ethylene. At high pressure, there is little change in intensity of the peak corresponding to π-bonded ethylene; however, there is a drop in intensity of other spectral features including ethylidyne. Also two ethyl peaks were visible. The turnover rate measured for ethane formation was 61 ± 3 molecules per platinum site per second. At lower pressures of hydrogen and ethylene, the surface had nearly a saturation coverage of ethylidyne from the onset of reaction with only a small concentration of di-σ bonded ethylene present. As the reaction continued, the di-σ bonded ethylene peak slowly disappeared, and after 200 min the only spectroscopic feature present was from ethylidyne. The turnover rate was 1.6 molecules per platinum site per second (i.e. did not change with the observed decrease in concentration of di-σ bonded ethylene). The π-bonded ethylene species could not be observed under these circumstances presumably because its concentration was too low.

We propose a model in which hydrogen dissociatively chemisorbs on a clean or ethylidyne-covered platinum surface (Fig. 3). This step is followed by the physisorption of ethylene on single atom sites to form π-bonded ethylene. If ethylidyne is present, it may move out of the way in order to accommodate the adsorption of the π-bonded ethylene. Although the two species reside in different sites, this may be necessary because of steric hindrance. Physisorbed ethylene is then hydrogenated in steps through an ethyl intermediate to ethane. All steps up to the incorporation of the second hydrogen are reversible.

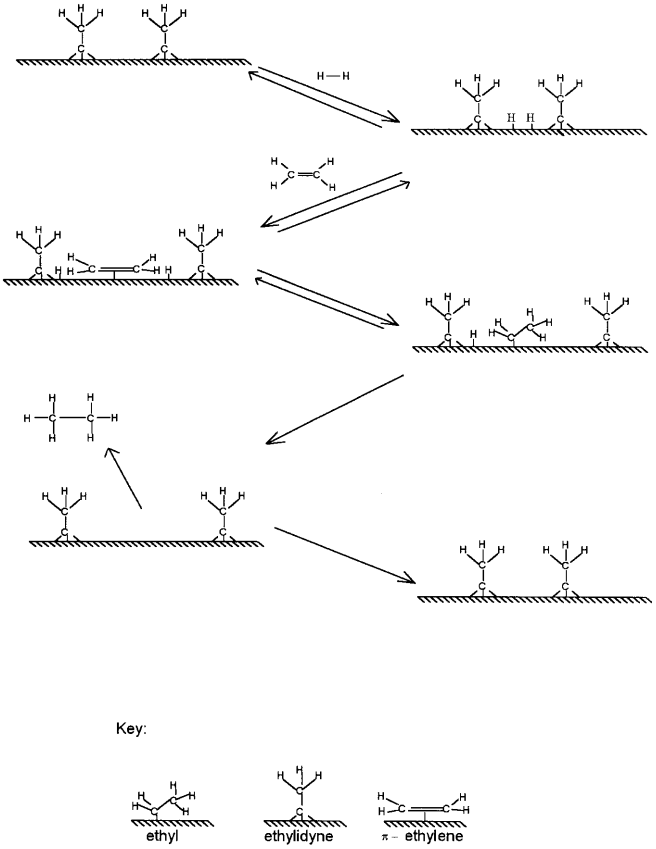

Fig. 3. Proposed mechanism for ethylene hydrogenation on Pt(111)

2.2 *Cyclohexene dehydrogenation and hydrogenation on* Pt(111) [20, 21]

The hydrogenation and dehydrogenation reactions of cyclohexene on Pt(111) crystal surfaces were investigated by surface vibrational spectroscopy via SFG both under vacuum and high-pressure conditions with 10-Torr cyclohexene and various hydrogen pressures from 30 Torr up to $\sim$ 600 Torr. At high pressures the gas composition and turnover rate (TOR) were measured by gas chromatography.

2.2.1 Cylcohexene dehydrogenation in vacuum at low and saturation coverage. The SFG spectrum at saturated coverage and at low temperature of *c*-C_6H_{10} on the Pt(111) surface is shown in Fig. 4a. At 130 K, the 2875 cm^{-1} and 2958 cm^{-1} features of CH_2 groups and Fermi resonance of 2918 cm^{-1} [22] indicate that cyclohexene has a half-chair conformation as a free molecule (π/σ-cyclohexene). The SFG spectrum changed at 217 K with two peaks at 2860 and 2945 cm^{-1}, which fits very well to a di-σ cyclohexene species formed at this temperature, as proposed by others [23]. At 283 K a π-allyl *c*-C_6H_9 species shows up on the surface [23–25]. With further heating to 383 K, the disappearance of the spectral feature is due to the complete dehydrogenation of the

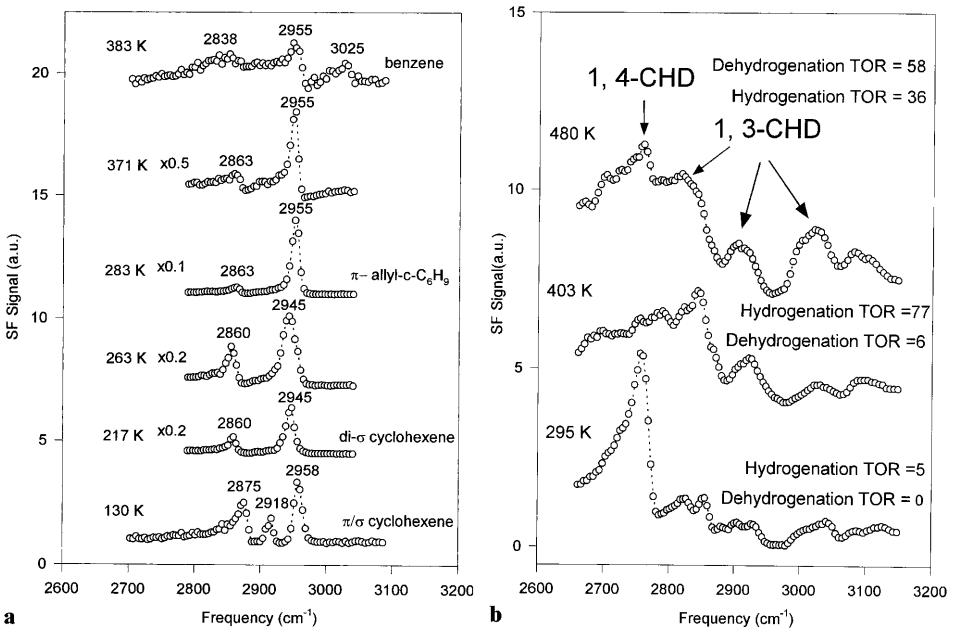

Fig. 4. a SFG study of cyclohexene thermal dehydrogenation at saturation coverage of cyclohexene on Pt(111) in the temperature range of 130–380 K in vacuum. **b** The temperature dependence of SFG spectrum during high pressure cyclohexene conversion on Pt(111) at 10 Torr cyclohexene/100 Torr hydrogen (The turnover rates (TOR) (number of molecules/platinum site/sec) are also indicated in the figure)

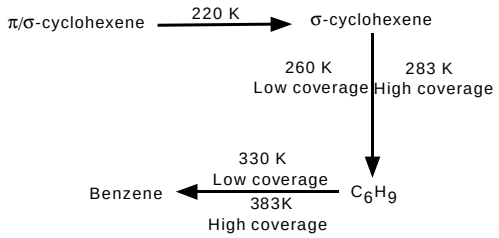

Fig. 5. Proposed reaction pathway of cyclohexene dehydrogenation in vacuum

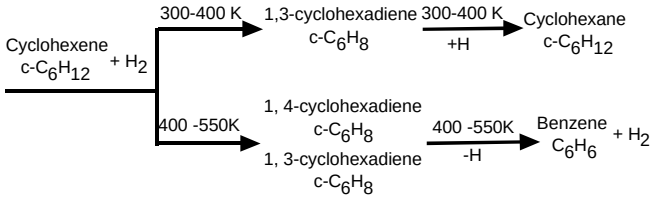

Fig. 6. Reaction mechanism of cyclohexene hydrogenation and dehydrogenation at high pressure

surface species to benzene [23], which is invisible on metal surface by the SFG technique. The SFG spectrum at low coverage and at low temperature of *c*-C_6H_{10} on Pt(111) surface shows only slightly differences. Based on the above discussion, the reaction pathway in Fig. 5 can be proposed.

2.2.2 Hydrogenation and dehydrogenation reactions of cyclohexene at high pressures. The high-pressure-reaction studies were carried out typically at 10 Torr pressure of cyclohexene with various hydrogen pressures up to 600 Torr in the temperature range of 300–560 K. The strong peak at 2765 cm^{-1} of 295 K spectrum (Fig. 4b) was attributed to 1,4-CHD (cyclohexadiene) on the surface and the weak peaks in the spectrum were from 1,3-CHD [26]. Interestingly, there was no evidence for the presence of C_6H_{10} and *c*-C_6H_9 species on the surface, which are the important species in chemisorbed cyclohexene dehydrogenation in vacuum. Above 300 K, 1,3-CHD became stronger and dominated the spectrum. The vibrational SFG spectrum remains unchanged in the temperature range of 300 to 400 K and hydrogenation is the only detectable reaction in this temperature range. Further increase in the surface temperature results in a decrease in the hydrogenation rate and an increase in the dehydrogenation rate and the presence of both 1,3- and 1,4-CHD on the surface. The simultaneous observation of the reaction kinetic data and the chemical nature of surface species allows us to postulate a reaction mechanism at high pressure: cyclohexene hydrogenates to cyclohexane via a 1,3-CHD intermediate, and dehydrogenates to benzene through both 1,3-CHD and 1,4-CHD intermediates (see Fig. 6).

2.3 High-pressure CO *oxidation on* Pt(111) [27, 28]

2.3.1 High-pressure CO *chemisorption on* Pt(111). High-pressure chemisorption of CO on Pt(111) at 295 K was studied by SFG surface vibrational spectroscopy (Fig. 7). Under UHV conditions, two CO species were present, giving rise to peaks at 1845 cm^{-1} and 2100 cm^{-1}, which can be attributed to CO adsorbed at bridge sites and atop sites, respectively [29–32]. The peak at 1845 cm^{-1} is weak compared to the one at 2100 cm^{-1}, because of the small IR and Raman cross sections and the broad peak width at room temperature for CO at bridge sites [33]. When the CO pressure was increased to 1 Torr, the bridge-bonded CO was no longer observable and the frequency of atop species shifted to 2105 cm^{-1}, which is due to the enhancement of dipole coupling between adsorbed CO molecules as the increasing CO coverage increased their packing density [34], thereby weakening their bonds to the metal. Further increase of the CO pressure resulted in a decrease of the intensity of the atop CO and a new peak at 2045 cm^{-1} together with a broad background became visible. The spectrum can be explained by the formation of an incommensurate overlayer of CO and perhaps also some terminally bonded CO at distorted or defect sites ($Pt(CO)_n$, $n > 1$).

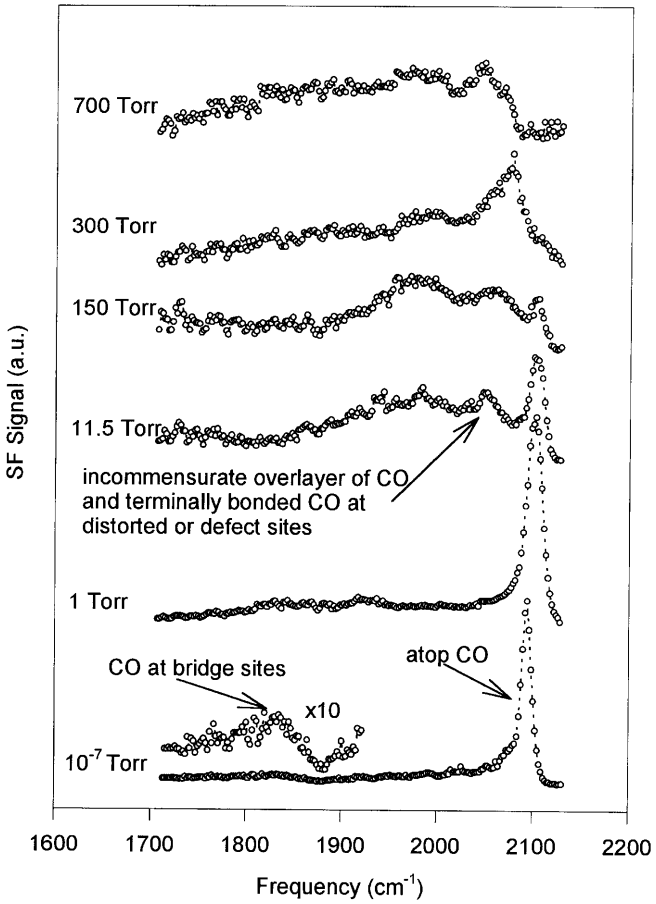

Fig. 7. Pressure dependence of SFG spectra of CO on Pt(111) at 295 K under various CO pressure

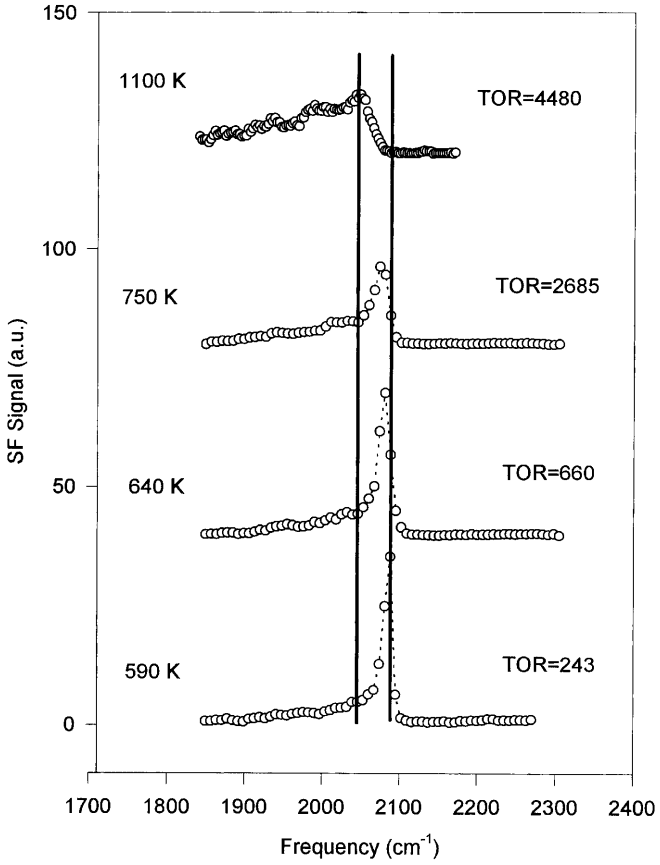

Fig. 8. Temperature dependence of SFG spectra of high pressure CO oxidation on Pt(111) under 40 Torr O_2/100 Torr CO/600 Torr He. The CO_2 turnover rate (TOR) for each temperature is also indicated

2.3.2 High-pressure CO *oxidation on* Pt(111). The in situ SFG spectra during reaction with 100 Torr CO/40 Torr O_2/600 Torr He (i.e. CO in excess) at various temperatures are shown in Fig. 8. The CO oxidation reaction was also investigated with the relative partial pressure of CO/O_2 greater than unity. These high-pressure studies of CO oxidation on Pt(111) using SFG spectroscopy reveal that there are two different reaction regimes: below and above ignition. Below the ignition temperature, atop CO dominates the spectrum. The reaction has an apparent activation energy of 42 kcal/mol, which is close to the desorption energy of atop CO, indicating that desorption of atop CO is the rate-limiting step. The reaction rate is inversely proportional to the atop CO concentration, suggesting that atop CO plays the role of an inhibitor in the reaction. Above the ignition temperature, atop CO becomes hardly detectable and the activation energy reduces to 14 kcal/mol, which is the reaction energy barrier of the oxidation reaction of CO and O on Pt(111). In both cases, the active CO species in the reaction are identified as those adsorbed at non-registry sites or carbonyl cluster-like species. The reaction rate appears to increase linearly with the surface concentration of such species.

2.4 Ethylene and CO *chemistry on* Rh(111)

It would be interesting to compare the chemisorption and catalytic chemistry over Rh(111) for the same molecules that were studied by using the Pt(111) surface. These two hexagonal surfaces exhibit similar behavior in the hydrogenation reaction of olefins and oxidation of carbon monoxide.

The SFG spectrum of ethylene on Rh(111) is different from that of Pt(111). No spectral feature was seen after the clean Rh(111) surface was exposed to ethylene at 140 K and three features were observed at 2892 (ethylidyne) and 2921 and 2960 cm^{-1} above 180 K. Ethylidyne is the only species detected by SFG during high-pressure hydrogenation. The π-bonded species, the active species found on Pt(111), is undetectable because the higher nonresonant background of Rh(111) covers up the weak signal.

Figure 9 shows the SFG spectra of CO on Rh(111) at different pressures. The spectra are different as compared to CO on Pt(111) (Fig. 7): 1870 cm^{-1} for CO bound to multiple coordinated site and 2080 cm^{-1} for atop CO. With the increase of CO pressure, the intensity of the multiple-bonded CO increases slightly and the atop CO intensity, on the other hand, decreases. Decomposition of CO on clean Rh(111) occurs above 750 K because the SFG spectral intensity of CO decreases above this temperature. However, CO behaves much differently on a Rh(111) surface with defects, which were introduced by Argon-ion bombardment. The defects on the Rhodium surface are much more active to break the C = O bond so that the spectral features of CO disappeared at temperatures higher than 600 K.

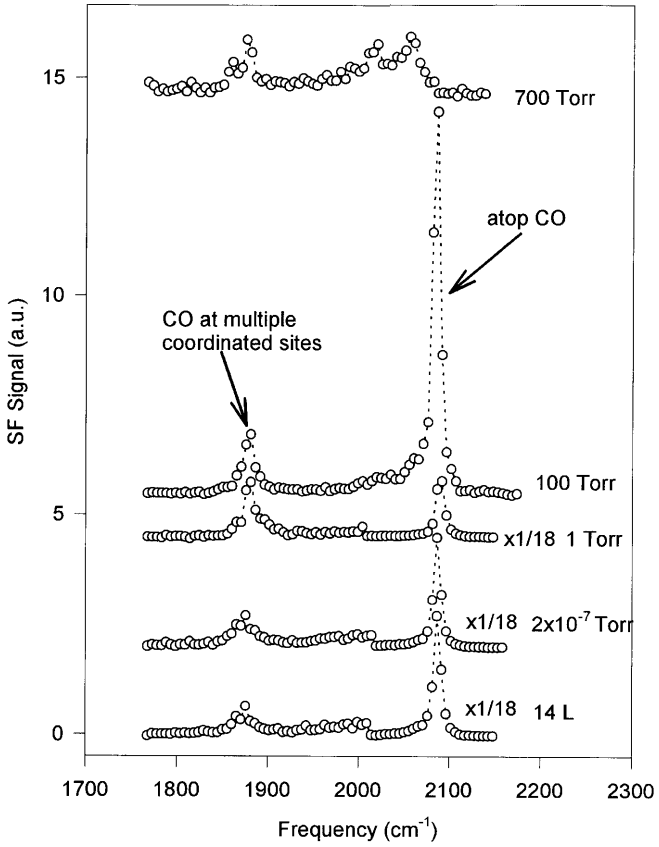

Fig. 9. SFG spectra of CO on Rh(111) at different pressure with a ordered structure formed in UHV

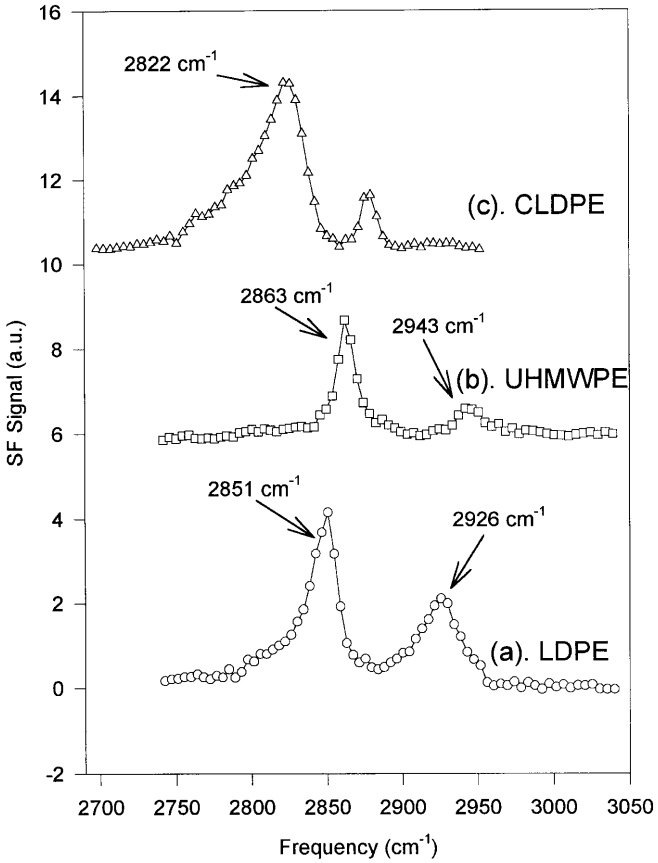

Fig. 10. SFG spectra of low density (a), and ultrahigh molecular weight (b), and commercial low density (c), polyethylenes, with ssp (for SF output, visible input, and IR input) polarization combinations

2.5 Studies of surface structures and compositions of polyethylene and polypropylene [35, 36]

2.5.1 Polyethylene. The IR and Raman spectra of the three types of polyethylene, a low-density polyethylene (LDPE), an ultra-high-molecular-weight PE (UHMWPE) and a commercial low-density PE (CLDPE), are identical and consistent with the published results for polyethylene [37, 38]. But their SFG spectra are markedly different, indicating that they have very different surface structures (Fig. 10). For LDPE (Fig. 10a), the band at 2851 cm^{-1} correlates well with the CH_2 symmetric stretch and the band at 2926 cm^{-1} can be assigned to the CH_2 asymmetric stretch [37, 38]. However, for UHMWPE (Fig. 10b), the symmetric and antisymmetric CH_2 stretching peaks shift to higher frequencies, which indicates that there are more gauche conformers in the polymer surface [39, 40]. The crystalline phase of polyethylene is composed of thin lamellae, about 10 nm thick, extending up to $1 \sim 10$ mm. The most striking feature of these lamellae is that while the molecular chains may be as long as $1 \sim 10$ mm, the direction of the chain axis is across the thickness of the platelet. This means that the chain must fold repetitively at the crystal surface, a phenomenon called chain folding. The folding surface must then contain a high density of gauche conformers, as required by the folding geometry. So we propose that the UHMWPE surface comprises mainly orderly packed gauche conformers, corresponding to the folding surface of the lamella. The 42° average orientation of the methylene group arises from spreading of the CH_2 groups at the surface because of chain folding. In the case of low-density polyethylene (LDPE), the trans-like peaks at 2851 and 2926 cm^{-1} indicate that mostly trans conformers exist at the polymer surface. The random packing of the polymer chains and the disorder of the polymer surface are evidenced by the larger bandwidths of the peaks in the SFG spectrum. The polarization measurements show an average orientation of 55° for the CH_2 groups. The SFG spectrum of CLDPE (Fig. 10c) is very different from those for LDPE and UHMWPE. The most striking feature is the disappearance of the CH_2 stretching peaks due to polyethylene, and the appearance of two new bands at 2822 and 2880 cm^{-1}. These two peaks are characteristic for the methoxy group (OCH_3), according to the surface vibrational study by Miragliotta et al. [41] and other vibrational studies of this chromophore [42]. These indicate that this commercial polymer surface is dominated by methoxy-contained species rather than polyethylene. It is known that stabilizers are commonly added to the industrial polyolefin products and these additives often contain methoxy moiety. The amount of additives is so small that they cannot be detected by IR and Raman spectroscopies, but they prefer to be segregate to the surface, due to their low surface energy [43], as evidenced by their dominant vibrational features in the surface-specific SFG spectrum.

2.5.2 Polypropylene. The IR and Raman spectra of the three types of polypropylene, an isotactic polypropylene (IPP), an atactic polypropylene (APP) and an industrial isotactic

polypropylene (CIPP) sample, are very similar. Their SFG spectra are quite different, showing that they have different surfaces. As with the industrial polyethylene sample, the industrial isotactic polypropylene surface is also covered by additives. The SFG spectra of APP suggest that at the APP surface, the hydrocarbon backbone tends to lie parallel to the surface with the methyl groups projecting out, which agrees well with the theoretical simulation of the APP surface [44]. The surface methyl groups of APP tend to point toward the interface in order to lower the interfacial energy while the surface polymer backbones lie flat to optimize their interaction with the underlying chains. Unlike APP, the methyl groups of IPP are restrained to the same side of the polymer chain. It has been well documented [45] that for IPP, in order to reduce steric interaction, CH_3 side groups are arranged in a staggered fashion, thus generating a 3_1 helix with a $(TG)_3$ conformation. Our measurements of orientation of CH_3 ($\sim 55°$ from the surface normal) and CH_2 ($\sim 58°$) are consistent with this IPP surface structure.

2.5.3 Temperature dependence of the polypropylene surface structure. SFG was also used to probe the glass transition of the polypropylene surface by taking spectra as a function of temperature, while cooling down the polymer in vacuum pressures of 10^{-5} Torr. The glass transition temperature of the bulk polymer occurs between 0 and $-20\,°C$ [46]. Figure 11a shows the SFG spectra obtained on atactic polypropylene (APP) above and below the glass transition. An increase in the ratio of the symmetric stretch of the CH_2 group to that of the CH_3 group in both APP and isotactic polypropylene (IPP) is observed as it is cooled through the glass transition. The square root of this ratio is plotted in Fig. 11b at different temperatures for both IPP and APP. The increase in the ratio of these two peaks is indicative of a reorientation of the CH_2 and CH_3 groups at the surface, as the polymer undergoes the glass transition. The glass transition occurs only in the amorphous phase, i.e. the crystalline part of the polymer is unaffected during the transition [45]. APP is amorphous (percentage crystallinity $< 5\%$) [47] whereas IPP is only partially amorphous (percentage crystallinity $> 60\%$) [47]. Hence the changes occurring during the transition are expected to be more pronounced in APP than in IPP, and this is what we see.

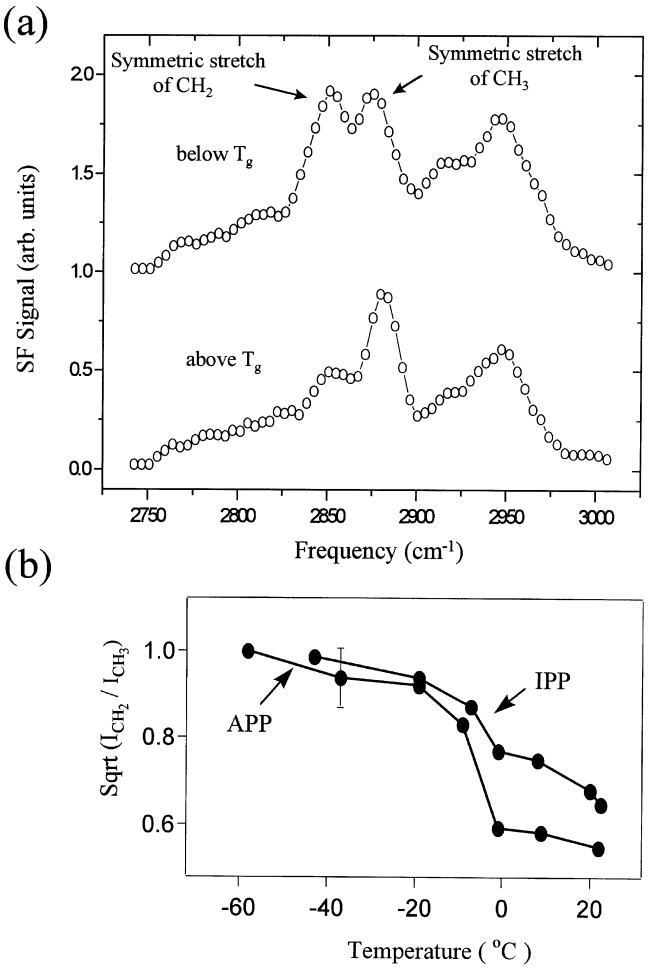

Fig. 11. a SFG spectra of atactic polypropylene above and below the glass transition temperature (T_g). As can be seen there is an increase in the ratio of the symmetric stretch of the CH_2 group relative to that of the CH_3 group below the glass transition. **b** The square root of the ratio of these two peaks at 2846 cm^{-1} and 2880 cm^{-1} plotted as a function of temperature for both isotactic (IPP) and atactic (APP) polypropylene. The increase in the ratio through the glass transition is larger for APP than for IPP

2.6 *Polymer blends* [48, 49]

Polymer blends are used widely as a means of tailoring the bulk and the surface properties of polymeric materials for various industrial and biomedical applications [50, 51]. The surface properties of three polymer blends were studied by using a combination of surface-sensitive techniques: sum-frequency generation (SFG), contact angle goniometry, X-ray photoemission spectroscopy (XPS) and atomic force microscopy (AFM). The three polymer blends studied are: Biospan-SP/Phenoxy base polymer (BSP/PHE), Biospan-S/Phenoxy base polymer (BS/PHE) and Biospan-F/Phenoxy base polymer (BF/PHE). Biospan-S and Biospan-F are polyurethanes capped with poly(dimethylsiloxane) (PDMS) and fluorocarbons ($-(-CF_2-)_n-$) as end groups. Biospan-SP has a similar structure to that of BS, but with 30% poly tetramethylene oxide (PTMO) in polyurethane replaced by poly ethylene oxide (PEO). The molecular structures of all the polymers are shown in Fig. 12. The surface tensions of BSP, BS, BF and PHE are 26, 22, 16 and 45 dyne/cm, respectively. The BSP, BS and BF work as surface-active polymers to protect the polymer blend surfaces in BSP/PHE, BS/PHE and BF/PHE. We find that the surface of the blend is sensitive to: (a) the bulk concentrations, (b) the surface energy of the surface-active polymer in the blend, and (c) the chemical environment.

2.6.1 Effect of bulk concentrations. The SFG results show that in air the polymer blend surface of BSP/PHE is totally covered by BSP when its bulk concentration is only 3.5 wt. %, while for BS/PHE and BF/PHE, even lower bulk concentrations of 1.7 wt. % BS and 1 wt. % BF completely cover these two blend surfaces. The blend surfaces are covered by Phenoxy when the bulk concentrations of BSP, BS and BF are lower than 0.25, 0.17 and 0.0625 wt. %, respectively. In the intermediate bulk concentrations of BF (0.0625 to 1 wt. %), BS (0.17 to 1.7 wt. %) and BSP (0.25 to 3.5 wt. %), the surface compositions of these three polymer blends change in a step-wise manner (SFG spectra of

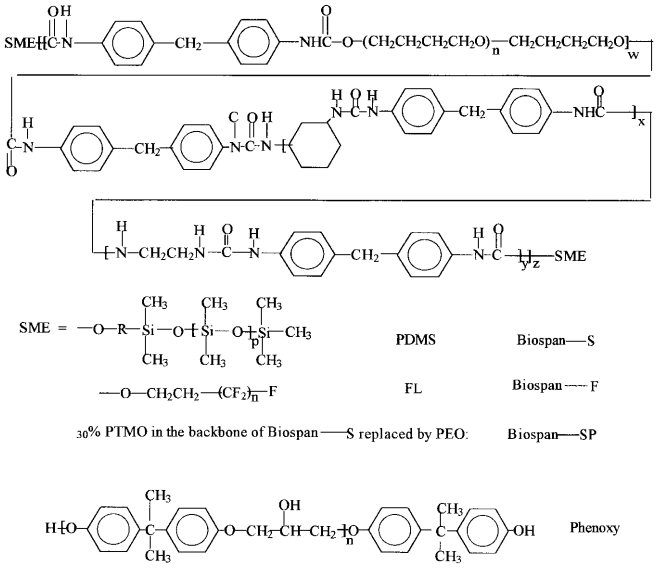

Fig. 12. Molecular structures of Biospan-S (BS), Biospan-F (BF), Biospan-SP (BSP) and Phenoxy (PHE)

BS/PHE are shown in Fig. 13 as examples). The contact angle measurement and the XPS show compatible results to SFG. From AFM measurements, we find that below 0.17 wt. % of BS in PHE, the surface morphology of the polymer blend is very similar to that of pure PHE; while above 1.7 wt. %, it resembles that of pure BS. Between 0.17% and 1.7% there appears to be a phase separation of BS and PHE into individual domains at the surface.

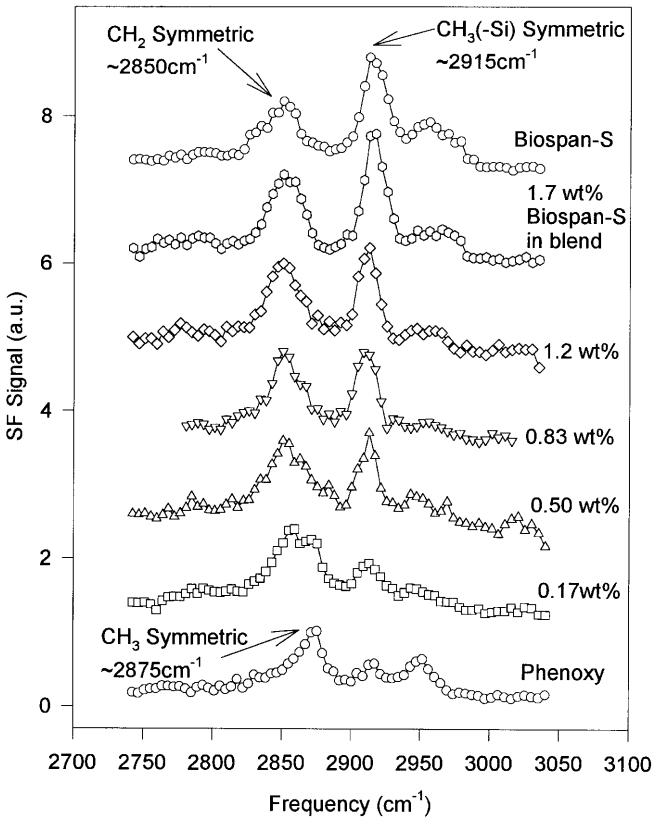

Fig. 13. SFG spectra of pure PHE, pure BS and BS/PHE blends as a function of BS bulk concentration in wt. %

2.6.2 Effect of the surface energy of the surface active agent. The comparison of BSP/PHE, BS/PHE and BF/PHE polymer blend surfaces shows that the lower the surface energy of the surface active polymer is (surface tension: BF < BS < BSP), the easier it is for it to cover the polymer blend surface (the minimum bulk concentration to cover the whole blend surface: BF (1 wt. %) < BS (1.7 wt. %) < BSP (3.5 wt. %)).

2.6.3 Effect of chemical environments. The polymer blend surfaces can reconstruct after contacting with water, and different blend surfaces behave in different ways. SFG results show that the surface BSP layer in BSP/PHE blend with 3.5 wt. % BSP bulk concentration will reorient after contact with water, which is similar to the change of the pure BS polymer surface after transferring from air to water: the hydrophobic silicon tail migrates into the bulk as the hydrophilic polyurethane backbone covers the surface [52]. BF/PHE blend with 1 wt. % BF bulk concentration on contact with water causes PHE to replace BF, which dominates the surface in air. But BF can completely cover the surface of BF/PHE blend with 5 wt. % BF bulk concentration both in air and water.

3 Conclusions

SFG bridges the gap between UHV and the high-pressure-reaction surface studies, and provides information on the structure of polymer surfaces in different chemical environments at the molecular level. SFG studies of ethylene hydrogenation show that π-bonded species on Pt(111) are the key intermediates. A model was proposed and can explain all the experimental results. π/σ and di-σ bonded cyclohexene and c-C_6H_9 species are the reaction intermediates for cyclohexene dehydrogenating to benzene in vacuum on the Pt(111) surface. At high pressures, cyclohexene hydrogenates to cyclohexane via a 1,3-CHD intermediates, and dehydrogenates to benzene through both 1,4-CHD and 1,3-CHD intermediates. The vibrational spectrum of CO on Pt(111) was monitored over 13 orders of magnitude in CO pressure by SFG and shows that different CO surface species exist at low and high pressures. High-pressure studies of CO oxidation on Pt(111) using SFG reveal that there are two different reaction regions: below and above ignition. Different CO surface species were detected in the two regimes. On the Rh(111) surface, different surface chemistries were observed as compared to Pt(111) during ethylene hydrogenation and CO adsorption.

The different SFG spectra of three different polyethylenes show their differences in their surface structure and composition: LDPE has more trans CH_2 on the surface, while the surface of UHMWPE has more gauche foldings and the additives aggregate on the CLDPE surface. From temperature-dependent measurements on the polypropylene surface we observe molecular orientational changes taking place on the polymer surface during the glass transition, and SFG is a viable tool for studying such changes. SFG studies of polymer blend surfaces correlate with AFM, XPS and contact angle measurements very well. More hydrophobic surface-active polymers will cover the polymer blends surfaces in air even

when their bulk concentrations are very low. The polymer blend surface composition can change when in contact with water.

Acknowledgements. We would like to thank Dr. P. Cremer, Dr. X.C. Su and Dr. D. Zhang in the SFG measurements and Prof. Y.R. Shen for all his great help. This work was supported by the Director, Office of Energy Research, Office of Basic Energy Sciences, Materials Science Division, of the US Department of Energy under Contract No. DE-AC03-76SF00098.

References

1. D. Woodruff, T. Delchar: *Modern Techniques of Surface Science* (Cambridge University Press, Cambridge 1986)
2. G.A. Somorjai: *Introduction to Surface Chemistry and Catalysis* (Wiley, New York 1994)
3. Y.R. Shen: *The Principle of Nonlinear Optics* (Willy, New York 1984)
4. Y.R. Shen: Nature **337**, 519 (1989)
5. Y.R. Shen: Annu. Rev. Phys. Chem. **40**, 327 (1989)
6. Y.R. Shen: Surf. Sci. **299**, 551 (1994)
7. P.S. Cremer, X.C. Su, G.A. Somorjai, Y.R. Shen: J. Mol. Catal. **131**, 225 (1998)
8. W.J. Feast, H.S. Munro, R.W. Richards: *Polymer Surfaces and Interfaces II* (Wiley, New York 1993)
9. M. Garbassi, E. Occhiello: *Polymer Surfaces: from Physics to Technology* (Wiley, New York 1993)
10. K.B. Lewis, D.R. Ratner: J. Colloid Interface Sci. **159**, 77 (1993)
11. F.M. Fowkes: *Contact Angle, Wettability, and Adhesion*, Advances in Chemistry Series 43, American Chemical Society (Washington DC 1964)
12. P. Guyot-Sionnest, J.H. Hunt, Y.R. Shen: Phys. Rev. Lett. **59**, 1597 (1987)
13. C. Hirose, N. Akamatsu, K. Domen: J. Chem. Phys. **96**, 997 (1992)
14. C. Hirose, H. Yamamto, N. Akamatsu, K. Domen: J. Phys. Chem. **97**, 10 064 (1993)
15. K.A. White, R.S. Ward, R.S. Gill, F. Lim, S.C. Coviello: *Surface Modification of Segmented Polyurethaneureas via Oligomeric End Groups Incorporated During Synthesis*, In *Surface Modification of Polymeric Biomaterials*, ed. by B.D. Ratner, D.G. Castner (Plenum, New York 1996)
16. P.S. Cremer, X.C. Su, Y.R. Shen, G.A. Somorjai: J. Am. Chem. Soc. **118**, 2942 (1996)
17. P.S. Cremer, X.C. Su, Y.R. Shen, G.A. Somorjai: Catal. Lett. **40**, 143 (1996)
18. T. Beebe, J. Yates: J. Am. Chem. Soc. **108**, 663 (1986)
19. J. Rekoske, R. Cortright, S. Goddard, S. Sharma, J. Dumesic: J. Phys. Chem. **96**, 1880 (1992)
20. X.C. Su, Y.R. Shen, G.A. Somorjai: submitted to J. Mol. Catal. A (1998)
21. X.C. Su, K. Kung, J. Lahtinen, Y.R. Shen, G.A. Somorjai: Catal. Lett. **54**, 9 (1998)
22. L. Lespade, S. Rodin, D. Cavagnat, S. Abbate: J. Phys. Chem. **97**, 6134 (1993)
23. F.C. Henn, A.L. Diaz, M.E. Bussel, M.B. Hugenschmidt, M.E. Domagala, C.T. Campbell: J. Phys. Chem. **96**, 5965 (1992)
24. D.P. Land, W. Erley, H. Ibach: Surf. Sci. **289**, 237 (1993)
25. R. Martin, P. Gardner, M. Tushaus, Ch. Bonev, A.M. Bradshaw, T.S. Jones: J. Electron Spectrosc. Relat. Phenom. **54**/**55**, 773 (1990)
26. X.C. Su, Y.R. Shen, G.A. Somorjai: Chem. Phys. Lett. **280**, 302 (1997)
27. X.C. Su, P.S. Cremer, Y.R. Shen, G.A. Somorjai: Phys. Rev. Lett. **77**, 3858 (1996)
28. X.C. Su, P.S. Cremer, Y.R. Shen, G.A. Somorjai: J. Am. Chem. Soc. **119**, 3994 (1997)
29. N.R. Avery: J. Chem. Phys. **74**, 4202 (1981)
30. W.D. Mieher, L.J. Whitman, W. Ho: J. Chem. Phys. **91**, 3228 (1989)
31. H. Steininger, S. Lehwald, H. Ibach: Surf. Sci. **123**, 264 (1982)
32. B.E. Hayden, A.M. Bradshaw: Surf. Sci. **125**, 787 (1983)
33. E. Schweizer, B.N. Person, M. Tushaus, D. Hoge, A.M. Bradshaw: Surf. Sci. **213**, 49 (1989)
34. A. Crossley, D.A. King: Surf. Sci. **68**, 528 (1977)
35. D. Zhang, Y.R. Shen, G.A. Somorjai: Chem. Phys. Lett. **281**, 394 (1997)
36. D.H. Gracias, D. Zhang, Y.R. Shen, G.A. Somorjai: to be published
37. D.O. Hummel: *Polymer Spectroscopy* (Verlag Chemie, London 1973)
38. P.A. Bentley, P.J. Hendra: Spectrochimica Acta Part A **51**, 2125 (1995)
39. R.G. Snyder, H.L. Strauss, C.A. Elliger: J. Phys. Chem. **86**, 5145 (1982)
40. M.J. Hostetler, J.J. Stokes, R.W. Murray: Langmuir **12**, 3604 (1996)
41. J. Miragliotta, R.S. Polizzotti, P. Rabinowitz, S.D. Cameron, R.B. Hall: Chem. Phys. **143**, 123 (1990)
42. N.B. Colthup, L.H. Daly: *Introduction to Infrared and Raman Spectroscopy* (Academic Press, New York 1994)
43. D.H. Gracias, D. Zhang, Y.R. Shen, G.A. Somorjai: Tribol. Lett. **4**(3–4), 231 (1998)
44. R.C. Spiker, I.W. Levin: Biochim. Biophys. Acta **338**, 316 (1975)
45. J.M.G. Cowie: *Polymers: Chemistry and Physics of Modern Materials* (Intext Eduational Publishers, New York 1981)
46. D. Zhang, D.H. Gracias, R. Ward, M. Gauckler, Y. Tian, Y.R. Shen, G.A. Somorjai: J. Phys. Chem. **102**(32), 6225 (1998)
47. B. Bogdanov, M. Michailov: *Properties of Polyolefins*, In *Handbook of Polyolefins*, ed. by C. Vasile, R. Seymour (Marcel Dekker, New York 1993) p. 314
48. Calculated from heats of fusion measured by Differential Scanning Calorimetry
49. Z. Chen, R. Ward, Y. Tian, A.S. Eppler, Y.R. Shen, G.A. Somorjai: to be published
50. B.R. Liang, L.H. Pan, X.J. He: J. Appl. Polym. Sci. **66**, 217 (1997)
51. C.D. Han: *Polymer blends and composites in multiphase systems*, Advances in chemistry series 206, American Chemical Society (Washington DC 1984)
52. D. Zhang, R.S. Ward, Y.R. Shen, G.A. Somorjai: J. Phys. Chem. **101**, 9060 (1997)